行政院國家科學委員會專題研究計畫　期中進度報告

晶體材料之載子自旋與同調聲子動力學之研究(1/3)

計畫類別：個別型計畫
計畫編號：NSC91-2112-M-009-037-
執行期間：91 年 08 月 01 日至 92 年 07 月 31 日
執行單位：國立交通大學光電工程研究所

計畫主持人：黃中垚

報告類型：精簡報告
報告附件：出席國際會議研究心得報告及發表論文
處理方式：本計畫可公開查詢

中　華　民　國 92 年 5 月 26 日

行政院國家科學委員會補助專題研究計畫期中進度報告

晶體材料之載子自旋與同調聲子動力學之研究(1/3)

計畫類別：v 個別型計畫　　□ 整合型計畫
計畫編號：NSC 91－2112－M－009－037－
執行期間：　91 年 8 月 1 日至 92 年 7 月 31 日

計畫主持人： 黃中垚
共同主持人：
計畫參與人員：

成果報告類型(依經費核定清單規定繳交):v 精簡報告　□完整報告

本成果報告包括以下應繳交之附件：
□赴國外出差或研習心得報告一份
□赴大陸地區出差或研習心得報告一份
v 出席國際學術會議心得報告及發表之論文各一份
□國際合作研究計畫國外研究報告書一份

處理方式：除產學合作研究計畫、提升產業技術及人才培育研究計畫、列管計畫及下列情形者外，得立即公開查詢
□涉及專利或其他智慧財產權，□一年□二年後可公開查詢

執行單位：交通大學光電工程研究所

中　華　民　國　92　年　5　月　31　日

中文摘要

此三年期計畫主要目標在應用飛秒雷射科技分析半導體電子自旋與鐵電晶體同調聲子動力學。我們將使用光波合成技術操控量子侷限材料體系之電子自旋與同調聲子。

在第一年進度報告裡我們呈現：(一)新波長飛秒雷射光源和極微弱光信號之全光場分析技術之發展。 我們未來的研究將奠基於這些儀器與技術之開發。(二) 為滿足量子侷限結構材料之研究需求, 我們也報導以溶液成長法製備之高螢光效能的半導體量子點和製備週期排列奈米線所需之自動組裝奈米結構模具。（三）藉飛秒反射穿透率量測技術我們也分析化學劑量比鈮酸鋰和銀 硫 硒 四 A1 對稱聲子, 和以時析富氏紅外光譜技術分析鐵電性液晶的電致轉向動態。 這些成果不但呈現我們在材料製備與分析技術方面的發展而且也展現我們的努力與為下一階段研究所做的準備。

Abstract

The main objective of this three-year research program is to apply femtosecond laser technologies for probing dynamics of carrier-spin transport in semiconductor and coherent phonon generation in ferroelectric crystal. By employing optical pulse shaping technique, we plan to further manipulate the coherence transport of the carrier spin and phonon generation in some quantum-confined systems.

In this first-year progress report, we shall present: (1) the developments of new femtosecond laser source and novel single-shot full-field characterization technique for analyzing extremely weak optical signal. Based on these developments we shall be able to pursue our further research. (2) To meet the research need of advanced materials with quantum-confined structures, we report our recent achievements in preparing highly luminescent semiconductor quantum dots from solution growth and self-organizing nano template for periodic array of nanowires. (3) Femtosecond differential reflectivity/transmission measurement technique was employed to probe the A1-symmetry optical phonons of home-grown stoichiometric lithium niobate, and quaternary $AgGaS_xSe_{1-x}$ crystals. We also apply time-resolved Fourier transform infrared absorption spectroscopy for investigating field-induced reorientation of ferroelectric liquid crystal mixture. These achievements not only show fruitful results of new characterizing techniques and materials preparations but also demonstrate our efforts and well preparation for the next stage research.

Progress Report

I. Development of new femtosecond laser source to meet the research demand of this project[1]

Tunable femtosecond pulses from the blue to the near UV region (<460 nm) are useful in many applications ranging from wide band-gap materials to biomolecules. Unfortunately, the tuning range of a 400-nm-pumped type-I BBO optical parametric amplifier only covers from 460-nm to 720-nm in the signal branch and from 900-nm to 2.4 μm in the idler. To solve the problem, we develop a tunable femtosecond source in the blue and near-UV region (from 380-nm to 465-nm) without using any

extra frequency-doubling crystal.

An output of an amplified Ti:sapphire laser is split into two parts: 90% of the energy is frequency-doubles to 405-nm with a 0.30-mm-thick BBO for pumping OPA. The rest 10% of the Ti:sapphire laser beam is used to generate white-light super continuum (WLS) with a 2-mm-thick CaF_2 plate. The generated WLS is collimated and then overlaps with the SH beam in a 2-mm-long type-I BBO cut at $\theta=29^o$. The beam crossing angle α between the seeding pulse and the pump is adjustable from 2 to 18 degrees. When the BBO is tuned to around the degenerate point of the OPA, a high-quality bright beam tunable from the near-UV to the blue was observed. The tunable short-wavelength radiation is attributed to a cascaded sum-frequency generation process from the OPA and the residual pump laser beam at 810-nm. With a pump energy of 80 μJ at 405-nm, the SFG yields tunable output from 380-nm to 465-nm with an energy of 9 to 11 μJ. The optical conversion efficiency from the pump-to-tunable SFG is more than 10%.

We found that when the seeding angle lies between 3 to 18 degrees, the phase-matching angle of the cascading SFG-OPA is coincidently overlapped with that of a 400-nm pumped type-I BBO OPA near the degenerate point. The central wavelength of the SFG is adjustable from 410 to 440-nm with the seeding angle. The central wavelength of the SFG becomes shorter at large seeding angle and longer at small seeding angle. When the seeding angle is fixed, the SFG can also be tuned by rotating the crystal. The tuning range covers from 380 nm to 460 nm. Figure 1 presents the theoretical calculation of the tuning range of the cascading SFG-OPA and the experimental results at different seeding angles.

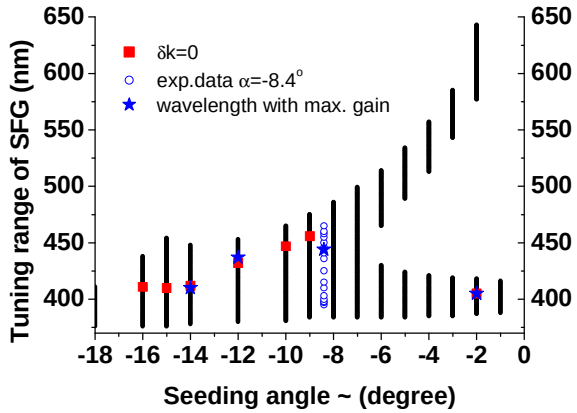

Fig.1. Theoretical tuning curves at various seeding angles α of SFG of OPA and residual 810-nm laser beam in a 400-nm pumped type-I BBO-NOPA. The black lines are the theoretical tuning curves at various seeding angles. The red squares are the calculated phase-matching points at the central wavelength of SFG and the star symbols denote the corresponding experimental data. The circles are the experimental tuning range at a seeding angle of 8.5 degree.

Using a newly developed OPA-based single-shot frequency-resolved optical gating (OPA-FROG) (see section II), we characterized the output of the OPA. Our

measured and retrieved OPA-FROG traces show that there is no significant chirping at the output of OPA and the pulse duration is about 75-fs. We also measured the FROG-trace of the SFG output and found that the pulse width of the generated SFG is longer than that of the OPA pulse but shorter than the 810-nm pulse, which agrees with that the tunable SFG pulse is a temporal convolution of the OPA and the residual fundamental beam.

II. Single-shot full field characterization of ultraweak femtosecond optical pulses[2]

To assist laser diagnosis and signal monitoring, we develop a novel full-field technique for characterizing ultraweak optical signal. The optical signal to be measured is first amplified by an optical parametric amplifier (OPA). The lowest detection level of the OPA-FROG is revealed to be about 100 atto joules. To prevent signal instability from persistent optical exposure on sample, we further improve our apparatus to possess single-shot detection capability. The resulting setup is shown in Fig. 2, which is very similar to the OPA used in Fig. 1 with some minor modifications.

The generated WLS is collimated by a parabolic mirror and then focused by a cylindrical mirror onto a BBO OPA. The pump beam at 400-nm is focused horizontally by a cylindrical mirrors into a vertical line. The two beams cross each other in the vertical direction as they travel through the BBO crystal.

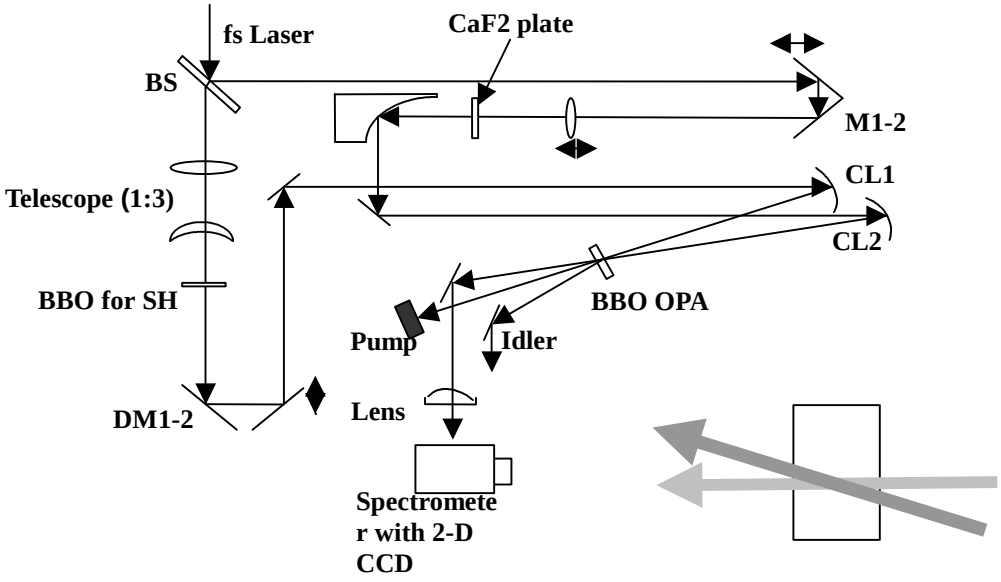

Fig. 2 Schematic setup of single-shot FROG for probing ultrashort optical field with ultraweak intensity using high-gain optical parametric amplifier

Here the strong pump beam acts not only as a gain provider for the weak signal but also as a gating to resolving the signal pulse. During the amplification process, the signal collides with the pump pulse in time domain and is sampled by the pump beam

along the vertical direction. The amplified signal was imaged onto the entrance slit of a spectrometer. Its spectral property is analyzed by the spectrometer and the vertical intensity distribution reveals the temporal profile information. The FROG trace was acquired with a 2-D CCD camera without scanning any mechanical delay line.

The single-shot OPA -FROG can be employed to measure optical pulse from the visible to the IR. The latter is seeded as the idler of OPA and then be characterized by measuring the corresponding signal pulse in the visible.

The apparatus described above can also be used to probe fairly complicated pulses. It has been shown that strong chirping can occur in WLS, which is notoriously known to be extremely unstable and non repetitive. Therefore its generation mechanism has not yet been fully understood. In Fig. 3 we present a single-shot OPA-FROG trace of a WLS field obtained with high pump intensity. Three temporal peaks and severe shear can be observed with our single-shot OPA-FROG, indicating a high degree of complexity in the WLS generation. The multiple-pulse profile can originate from multi-filament formation with high pump level, where each filament experiences different index of refraction from severe self focusing and nonlinear refraction effects.

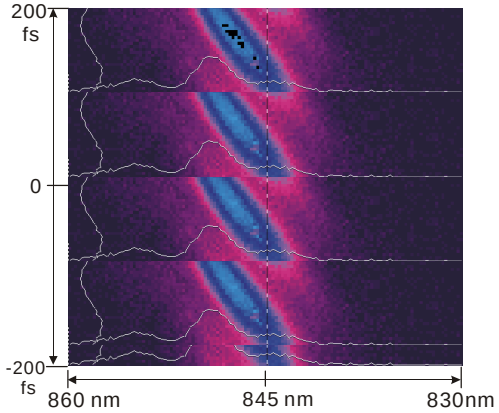

Fig. 3 Single-shot OPA-FROG trace of a highly chirped WLS pulse.

III. Development of novel preparation techniques of low-dimensional nanostructured materials

One of the major objectives of this research is to probe and control the carrier spin and phonon dynamics in low-dimensional quantum systems. Semiconductor quantum dots and periodic arrays of nanowires are the advanced material systems to be studies.

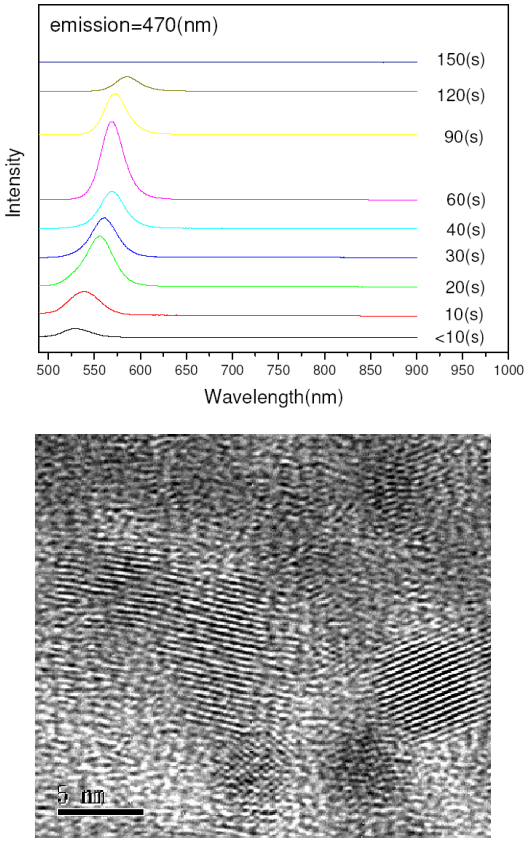

(a) (b)

Fig. 4(a: left) Fluorescent spectra of CdS quantum dots excited at 470 nm. These QDs are prepared with solution method by varying growth duration. (b: right) High resolution TEM clearly shows the regular atomic planes in these QDs indicating high crystal quality.

Semiconductor quantum-dots (QD) such as CdS from solution growth are able to achieve fluorescence quantum efficiency as high as 90%. Furthermore, their size distribution is very narrow and controllable with growth duration (see Fig. 4a). HRTEM measurement shows these solution-grown CdS QDs have very high crystal quality (see Fig. 4b). We are endeavored to develop a method for doping Mn ions into CdS for the study of quantum-confined spin transport dynamics.

We are also developing a preparation scheme for periodic arrays of nanowires in order to enhance application-related properties. Our approach combines selective growth/deposition with copolymer nanotemplate. We can demonstrate that with a proper thermal and solvent annealing, copolymer such as PS-b-PMMA can self organize into regular nanostructure. Fig. 5(a) presents a topographic image of PS-b-PMMA copolymer, which indicates highly-ordered triangular packaging can be formed. Fast Fourier transform pattern of Fig. 5(b) clearly shows a hexagonal symmetry of the film. To further enhance the self-forming order over a larger area, a well-planned scheme has to be developed in order to discover the optimum parameter set. We are preparing a *combinatorial library* on a silicon substrate with

micro-fabricated pattern to fulfill this purpose. The patterned substrate provides different conditions of surface chemistry and boundary force for better control on the self organizing process of Ps-b-PMMA template.

In brief, we are developing a novel technique for preparing highly-ordered nanostructured materials, which combines unique features of both bottom-up and top-down approaches. The PMMA-enriched areas in the resulting templates can be removed by etching to form nano column voids for selective material deposition. By invoking this unique approach, we are endeavored to prepare high density Co nanowire arrays for the next stage study.

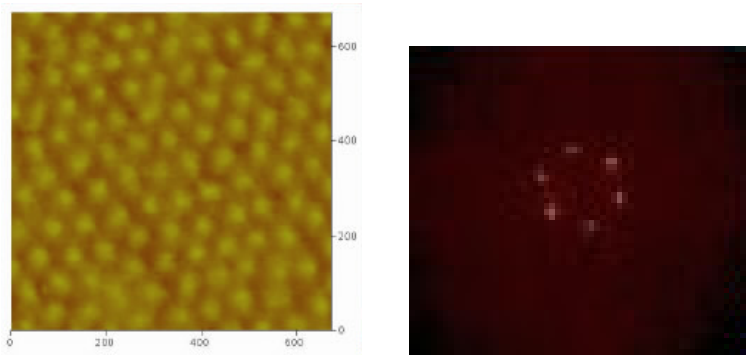

Fig. 5(a) Topographic image of PS-b-PMMA copolymer indicates highly-ordered triangular packaging configuration can self organize from a proper solvent annealing process. The circular spots denote the PMMA-enriched area. 5(b) The corresponding fast Fourier transform pattern of Fig. 5(a) clearly shows a hexagonal symmetry of the film.

IV. Phonon spectroscopy and dynamics of advanced optical materials

a. Stoichiometric lithium niobate crystal

Lithium niobate had been dubbed as the *silicon of optics* for quite a long time. It also has been widely uses in optic waveguide devices and photorefractive optics. Recently, periodically poled lithium niobate (PPLN) resurrects new interests of the material in laser applications. However, deficit of Li_2O causes a pinning effect of ferroelectric domains and therefore an extremely high poling field is required for reversing optic axis.

To reduce the deficit of Li_2O in a lithium niobate crystal, a stoichiometric growth method has to be developed. Recently, we had employed the knowledge of the phase diagram of Li_2O, K_2O, and Nb_2O_5 to successfully grow stoichiometric lithium niobate crystals. It had been shown that the UV cutoff wavelength (*i.e.*, the wavelength with an absorbance of 20 cm^{-1}) of lithium niobate strongly correlates with the atomic ratio of Li and Nb. We measured the UV cutoff edge and the plasma-excited atomic emission spectra and the results indicate our samples are indeed stoichiometric. This finding also agrees with the Curie-temperature measurements presented in Fig. 6. The Curie temperature of a pure congruent LiNbO3 (cLNB) crystal without MgO doping occurs at T_c=1148^{o}C (filled square),

while the Curie temperature of a pure stoichiometric LiNbO3 (sLNB, filled circle) is found to appear at T_c=1194 ^oC.

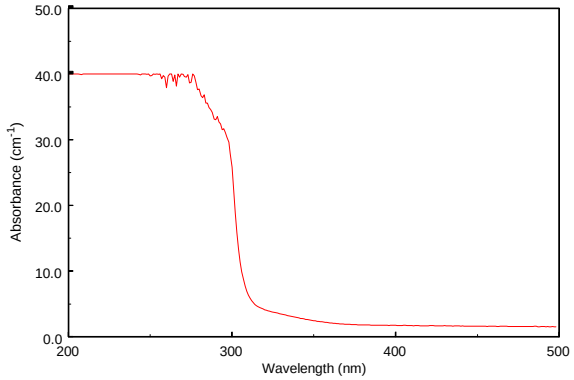

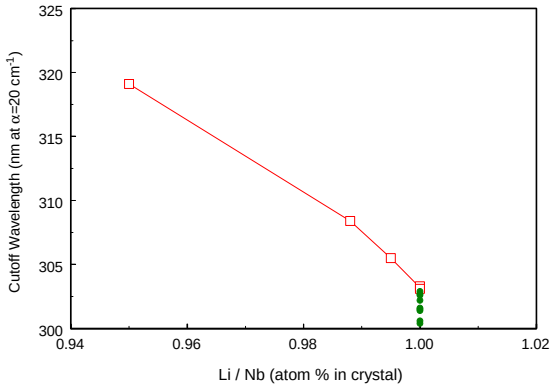

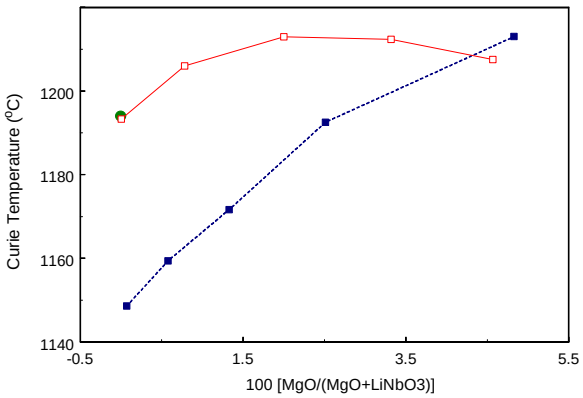

Fig. 6 (Top: left) Transmission curve of a stoichiometric lithium niobate (sLNB) crystal at the UV cutoff edge, (Top: right) the UV cutoff wavelength (the wavelength with an absorbance of 20 cm^{-1}) as a function of the atomic ratio of Li and Nb. The filled symbols are the data of our sLNB samples. (Bottom) Curie-temperature measurements of congruently grown LNB crystals (filled squares) and stoichiometric LNB (open squares) with varying doping level of MgO. The measured result of our pure stoichiometric LNB is presented by the filled circle, which has a Curie temperature of 1194 ^oC.

The low-temperature ferroelectric phase of $LiNbO_3$ is originated from a displacement Δz of the Li^+ ions along its optical axis. The lowest-energy phonon mode with A1-symmetry is attributed to the ferroelectric mode, which becomes significantly softening at the phase transition. It had been reported that the lowest-energy A1-symmetry phonon mode of $LiNbO_3$ crystal has a vibrational frequency of 250 cm^{-1} (7.5 THz). Note that all currently known displacement-type ferroelectric crystals follows empirical rules of $P_s=(258\pm9)\ \Delta z$ and $T_c=(2.00\pm0.09)\times10^4\ (\Delta z)^2$. Since unit-cell distortion from the A1 optical phonon excitation belongs to the same type of distortion from the ferroelectric-paraelectric phase transition, therefore it could be perturbed by Li_2O-deficiency in a congruently grown $LiNbO_3$ crystal. This was indeed observed by our differential transmission measurement with a femtosecond impulsive Raman excitation technique shown in Fig. 7. The optical transmission is modulated by the refractive index change from phonon excitation. The fast Fourier transform of the modulated transmission curve therefore reflects the phonon excitation spectrum. We detect a slightly blue shift from 250 cm^{-1} to 255 cm^{-1} for the A1-TO phonon mode in a congruently grown and a stoichiometric $LiNbO_3$. In view that for displacement-type ferroelectric crystals, $kTc=(1/2)K(\Delta z)^2$, where k is the Boltzman constant, and K denotes the force constant of the ferroelectric mode. Thus both of the Curie temperature and the A1-TO phonon frequency indicate a stronger force constant in the potential-energy curve of the Li^+ ion displacement along the optical axis of sLNB.

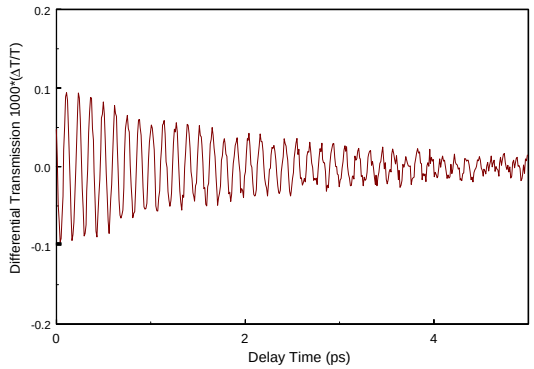

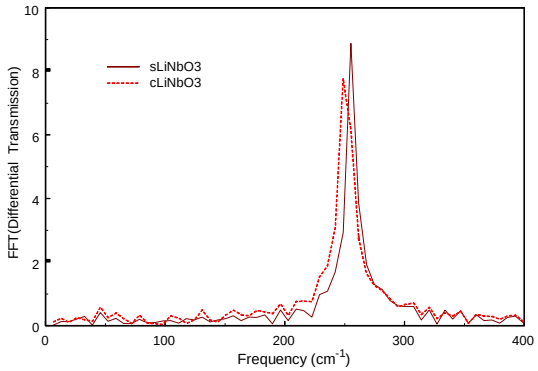

Fig. 7 (a) Differential transmission measurement on a c-cut stoichiometric LiNbO3 crystal plate with femtosecond impulsive Raman scattering excitation; (b) FFT of the differential transmission curves for a congruently grown (dashed) and stoichiometric (solid curve) LiNbO3 crystals.

b. Quaternary chalcopyrite $AgGa(S_xSe_{1-x})_2$ crystals[3]

Effects of cation substitution on optical and electronic properties had attracted numerous research interests of materials scientists. $AgGa(S_xSe_{1-x})_2$ crystals are solid solutions of the two infrared nonlinear optical crystals, $AgGaS_2$ and $AgGaSe_2$. We investigated the effects of cation substitution on these materials experimentally and theoretically. We found the bandgaps, optical properties, and bulk modulus are linearly dependent on the substitution concentration x of the cation S. The major effect of the cation substation can be understood via a change of unit cell volume.

From lattice dynamic calculation, we note that the lowest-energy A1 mode is associated with the relative motion of the cations (S or Se) along x- and y-axis. Therefore Se substitution, which increases the cell volume, shall also reduce the A1-mode phonon frequency. Indeed by measuring differential transmission with a femtosecond impulsive Raman excitation technique (see Fig. 8) we confirm that the A1-mode has a vibration frequency of 295 cm^{-1} for $AgGaS_2$ and 181 cm^{-1} for $AgGaSe_2$. The frequency down shift scales very well with effective mass. For the mixed crystals, the phonon frequency of A1 mode was found to linearly vary with the cation substitution concentration x. As a concentration near 50%, broader bandwidth of the phonon mode was also found, which can be ascribed to the substitution-induced disorder. Therefore a weaker amplitude and shorter lifetime of the A1-mode shall be observed.

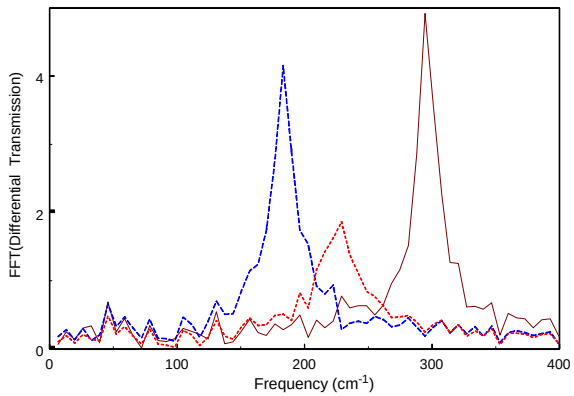

Fig. 8 Vibration spectrum of A1 phonon of $AgGaS_2$ (solid curve), $AgGaSe_2$ (dashed, blue) and mixed crystal of $AgGaS_{0.5}Se_{0.5}$ measured with femtosecond impulsive Raman excitation technique.

c. Field-induced re-orientation dynamics of surface stabilized ferroelectric liquid crystal mixture[4]

For this study, time-resolved measurements of electro-optical (EO) response and Fourier-transform infrared absorption (FTIR, see Fig. 9) of surface stabilized ferroelectric liquid (SSFLC) had been employed to deduce the sub molecular motion during field-induced reorientation process. We found that in steady state all FLC molecules rotate in unison about the layer normal by an electrical field.

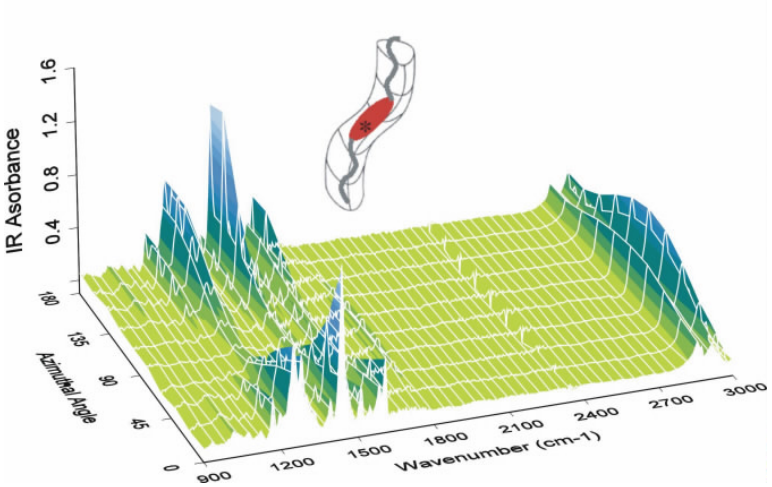

Fig. 9 FTIR spectra of an SSFLC measured without electrical applied field are plotted as a function of the angle between the incident IR polarization and the rubbing direction of the cell (*i.e.*, the X-axis).

At the transient condition, the angular motion of the FLC director was found to response rapidly to a pulsed driving field. However, the orientation distribution spreads out first and then slowly converges to the direction of the reoriented director (see Fig. 10). All the core segments momentarily reverse their rotating direction, and then relax to the steady-state direction with different speed (see Fig. 10). We conclude that the SSFLC molecules in the mixture can be viewed as an effective rigid

unit when an external field is applied. But when the field is removed, the field-free relaxations of different segments are not in unison.

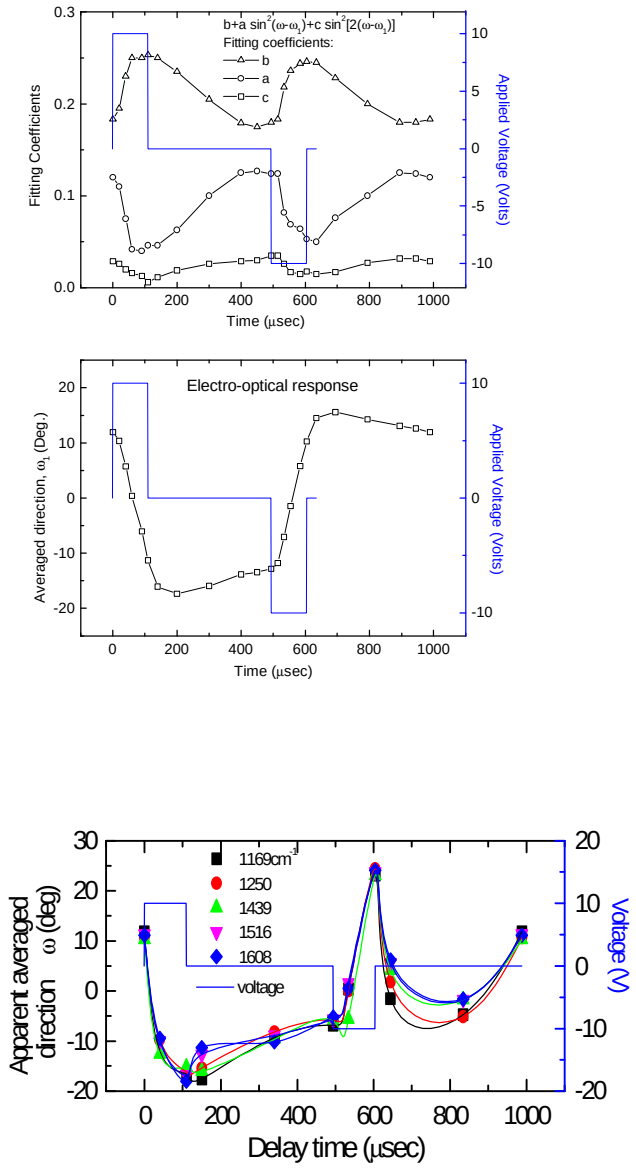

Figure 10 (Left: top) Fitting parameters (symbols) of the electro-optical azimuthal patterns and the applied voltage (solid line) are plotted as a function of time. (Left: bottom) The deduced orientation angle of the optic axis of FLC film is also shown as open squares. Rubbing direction of the FLC cell is along the 0 degree.
(Right) Transient orientations of several atomic segments associated with the FLC cores are presented as a function of delay time.

Related publication of this project

[1] C. K. Lee, J. -Y. Zhang[+], J. Y. Huang and C. L. Pan, *Generation of femtosecond Laser Pulses Tunable from 380 nm to 465 nm via cascaded Sum-Frequency Generation and Optical Parametric Amplification with a type-I Non-collinearly Phase Matched BBO Crystal*, submitted to *Optics Express*.
[2] Jing-yuan Zhang, Chao-Kuei Lee, Jung Y. Huang and Ci-Ling. Pan, *Single-shot XFROG measurement of extremely weak ultrashort optical pulses with a non-collinear beam-crossing optical parametric amplifier*, submitted to *Opt. Lett.*

[3] L. C. Tang, M. H. Lee, C> H. Yang, J. Y. Huang, and C. S. Chang, *Cation substitution effects on structural, electronic, and optical properties of nonlinear optical $AgGaS_xSe_{1-x}$ crystals*, submitted to J. Phys. C.
[4] Wen-Tse Shih*, Jung Y. Huang*, and Jing Y. Zhang^{+}, *Field-induced re-orientation dynamics of surface stabilized ferroelectric liquid crystal mixture*, submitted to *Liquid Crystal*.